**42nd AIAA Plasmadynamics and Lasers Conference
 in conjunction with the
 18th Internati**
27 - 30 June 2011, Honolulu, Hawaii

AIAA 2011-3740

Collision Modeling for High Velocity Ions
in a Quiescent Gas

Samuel J. Araki[*] and Richard E. Wirz [†]

University of California, Los Angeles, CA, 90095, USA

A particle-in-cell Monte Carlo collision model is developed to explore dominant collisional effects on high velocity ions incident to a quiescent gas, as examined in an ion gun experiment being carried out by UCLA researchers. Two different collision mechanisms are implemented in the computational model: elastic and charge exchange (CEX) collisions. Because of very low ionization level observed in the ion beam experiment, Coulomb collision is not incorporated in the model. The two collision types are approximated by two different models depending on incident particle energy: variable hard sphere model and classical scattering with repulsive interaction potential. The classical scattering model predicts a high probability in small angle scattering at large ion energies of interest. Four different species (The primary and CEX ions, fast neutrals, and secondary electrons) are tracked separately, and their destinations within a well-defined domain are determined. Predicted currents as a function of the test cell pressure are compared with electrode currents measured in the ion gun experiment. The simulation results agree well with the experiment up to test cell pressure of 1 mTorr. Below this test cell pressure, each primary ion experiences one or two collisions on average. The simulation result starts to digress from the experimental result as an increasing number of collisions are involved at higher pressures. The computational results suggest that the primary ion energy can be reduced significantly after many collisions, however, repulsive interaction potential is a good approximation only at high energies. Therefore, a better interaction potential function valid for lower energies is needed to resolve the disagreement.

Nomenclature

$\mathbf{v}$	Velocity, m/s	CEX	Charge exchange collision
b	Impact parameter, m	CM	Center of mass frame
d	Diameter, m	e	Electron
E	Ion energy, eV	el	Elastic collision
J	Current, A	i	Ion
m	Mass, kg	LAB	Laboratory frame
n	Density, $1/m^3$	max	Maximum value
P	Collision Probability	o	Neutral
r	Distance between colliding paricles, m	r	Relative value
R_m	Classical turning point, m		
V	Collision interaction potential energy, eV	*Symbols*	
v	Speed, m/s	α	Polar angle of v_r wrt inertial coord sys
x	Distance from the from aperture, m	β	Azimuth angle of v_r wrt inertial coord sys
		χ	Center of mass deflection angle
Subscripts		ΔJ_i	Primary ion current loss, A
0	Initial value	Δt	Time step, s
1	Incident particle	Γ	Ion beam flux, $1/m^2 s$
2	Target particle	γ	Post-collision azimuth angle relative to v_r

[*]Graduate Student, Mechanical and Aerospace Engineering, 420 Westwood Plaza Los Angeles CA 90095, and AIAA Member.
[†]Assistant Professor, Mechanical and Aerospace Engineering, 420 Westwood Plaza Los Angeles CA 90095, and AIAA Senior Member. wirz@ucla.edu

American Institute of Aeronautics and Astronautics

Ω	Solid angle, sr	*Superscripts*	
σ	Collision cross section area, m^2	$*$	Post collision

I. Introduction

AN ion beam experiment has been conducted to examine the behavior of ions accelerated into a target gas surrounded by electrodes.[1] In the experiment, a mono-energetic xenon ion beam of 1500 eV is guided by deflection plates and Einzel lenses to obtain a desirable beam shape before entering a cylindrical test cell shown in figure 1. Figure 1 shows four different electrodes at which current is measured; they are inner cylinder, exit plate, back aperture, and collector plate. The inner cylinder wall and exit plate are made of stainless steel. As background neutral pressure is increased in the test cell, the high energy xenon ions increasingly experience collisions with slow xenon neutrals. The collisional effects have been observed by the currents measured at the test cell electrodes during the experiment.

In plasma simulations, three types of computational models are often employed: a kinetic model, a fluid model, and a hybrid model in which one species is solved via fluid equations and other species is solved by a kinetic model. At very low neutral pressure, mean free path of the ions becomes larger than the length of the test cell so that Knudsen (Kn) number becomes greater than unity. In this regime, the continuum assumption in the fluid equation is violated[2] so that it becomes necessary to use a kinetic model to solve the problem. The two collisional mechanisms mentioned above have been implemented in many computational models. For example, Oh[3] developed a particle-in-cell (PIC) model for a Hall thruster plume and used variable hard sphere (VHS) collision method for ion-neutral elastic collision. In his model, the CEX collisions were simulated by simply switching the velocity vectors of the ion and neutral collision partners. The CEX collision has also been implemented in JPL developed ion optics code (CEX2D and CEX3D) to predict the erosion rate of the ion thruster accelerator grid caused by CEX ions impacting the grids.[4–6] Mikellides et al.[7] applied differential cross-sections computed classically for ion-neutral collisions to electrostatic thruster plume model using a LaGrangian fluid model and obtained a good agreement between the computational and experimental results for angular dependence of ion energy and flux.

The objective of this investigation is to develop a PIC Monte Carlo collision model that may be used to explore the collisional effects on plasmas during the experiment. The computational model will employ a domain and boundary condition that matches the well-defined "test cell" experimental domain as described in Ref. 1. Using matching domains will allow direct comparisons between computational and experimental results. This paper is organized as follows: the detailed description of the computational model is provided in section II. An analytical model to predict sum of the collector plate current and the back aperture current is given in section III. Results consisting of comparisons between measured and computed electrode currents are presented and discussed in section IV. The paper closes with some conclusions and future work in section V.
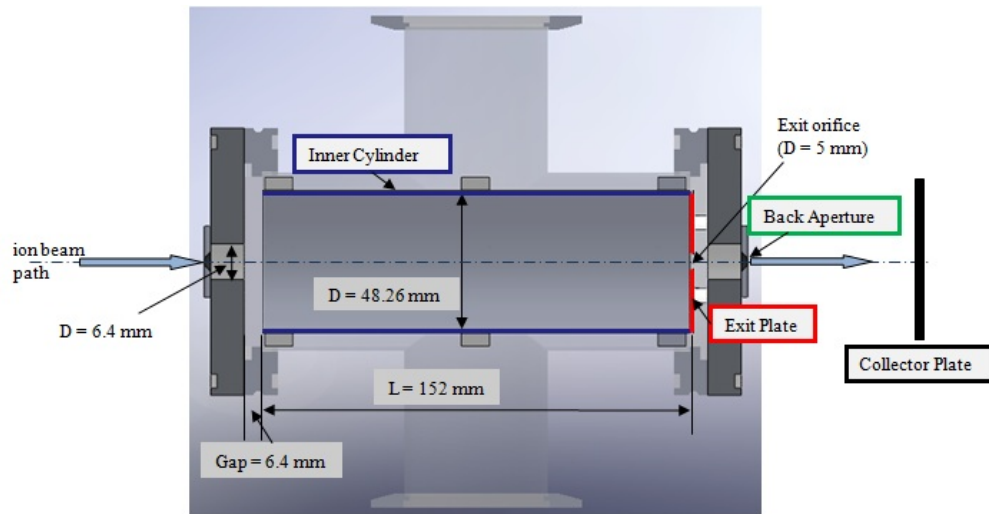

Figure 1. A cylindrical test cell used in the ion beam experiment

American Institute of Aeronautics and Astronautics

II.   Computational Model Description

A PIC Monte Carlo tracking and collision technique is employed in this computational model. The model consists of four sub-models:

- Potential solver
- Primary ion and CEX ion tracking
- Fast neutral tracking
- Secondary electron tracking

In the model, a high energy ion beam of 1500 eV (primary ions) enters the test cell and encounter background neutrals. Most of the primary ions can go through the test cell without experiencing any collision if the background pressure is low enough. As the background pressure is increased, probability of the primary ions colliding with neutrals increases, and a fraction of the ions experiences elastic collisions with neutrals. During the elastic collisions, the ions can exchange charges with neutrals to create slow CEX ions and fast neutrals.

When the primary ions and fast neutrals impact electrodes, secondary electrons can be emitted from the walls, affecting the currents measured at the electrodes. For the preliminary computational effort, several assumptions regarding of secondary electrons are made. The emission of secondary electrons is approximated to be at cosine distribution normal to the surface.[8] For the first order approximation, a constant secondary electron yield (SEY) of 0.2 is used. The SEY for the specific combination of xenon and stainless steel at an energy of 1500 eV is not found in any literature, therefore, the SEY is extrapolated from SEY values for combinations of proton and gold, proton and stainless steel, and xenon and gold at ion energy of 1500 eV.[9, 10] Also, a fraction of SEY due to incident neutrals and ions of 0.8 is used as the value less than unity is typical for ion energy less than 30 keV.[8] The secondary electron emission due to low-energy (< 0.1 eV) CEX ions is neglected because SEY at low energies is much lower than that for the high energy ions and neutrals.[8]

Figure 2.   Simplified flowchart for the computational model

Four different species (primary and CEX ions, fast neutrals, and secondary electrons) are tracked separately. For all the particle tracking sub-models, similar computational method is used. Macro-particles, each representing a fraction of the current, are tracked individually using leap-frog method.[11] In order to find densities for all the species, particles are distributed to computational nodes at every time-step using density conserving shape function given by Ruyten.[12] Short range Coulomb collisions between ions are less important compared to the two types of collisions for the range of ionization level found in the experiment ($< 10^{-5}\%$), thus the Coulomb collision mechanism is not incorporated in the model. Electric potential is calculated by solving Poisson's equation computationally using space charge distribution calculated from other sub-models. The four sub-models are ran multiple times until the electric potential reaches steady-state. Finally, electrode currents as a result of particle impacting the walls is output and compared with the experimental result. A simplified structure of the code is shown in figure 2.

A.   Collision Dynamics

Miller et al.[13] conducted guided-ion beam experiment to find measure $Xe^+ + Xe$ symmetric charge-exchange cross-section as a function of laboratory ion energy. In their experiment, all the ions (primary ions, scattered ions, and scattered CEX ions) are detected and distinguished by their separate arrival times. The measured cross-sections agreed well with earlier experiments. They provided a functional form of the cross section given as

$$\sigma_i = 10^{-20}(87.3 - 13.6 \log(E_r)) \tag{1}$$

At ion energy of 1500 eV, $\sigma_i = 44.1$Å. σ_i includes both cross sections for scattered primary and CEX ions. In order to incorporate the collisions to the computational model, it is necessary to distinguish the cross sections for scattered primary and CEX ions so that $\sigma_i = \sigma_{el} + \sigma_{CEX}$. For the preliminary effort, it is
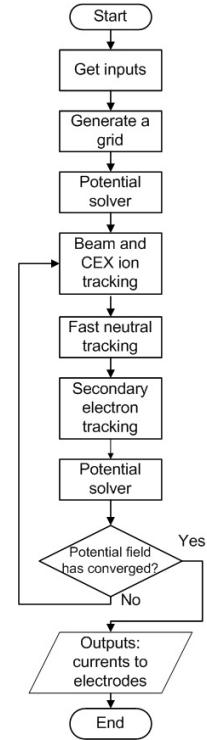
American Institute of Aeronautics and Astronautics

assumed that both the cross sections are equal, $\sigma_{el} = \sigma_{CEX} = \frac{1}{2}\sigma_i$. The same assumption is also used to derive an empirical model by Scharfe et al.[14] A more detailed discussion on collision cross sections is given in section II.C. Between one time-step, Δt, the probability that a particle experiences either an elastic or a CEX collision is expressed as follows:

$$P_{total} = 1 - \exp(-\Delta t \sigma_i v_i n_o) \tag{2}$$

Eq. (2) gives a positive value that is always less than or equal to 1. Whether a collision event takes place or not is determined by comparing Eq. (2) with an uniformly probable number between 0 to 1 generated by random number generator, $rand\#$. The random number is updated every time it appears in different equations. If $P_{total} > \text{rand}\#$, then the particle experiences either an elastic or CEX collision. By the assumption made for the collision cross section, 50 % of the particles is assumed to experience the CEX collisions out of all the paricle having collisions, and the primary ion current loss, ΔJ_i, by CEX collision is approximated by $\Delta J_i = 0.5 J_i$. The rest of the macro-particle current given by $J_i = J_{i0} - \Delta J_i$ experiences elastic collisions.

Because of the range of the test cell pressure varied during the experiment, the gas is dilute enough that each collision can be considered to involve only two particles. During an elastic collision, it is assumed that there is no interchange of translational and internal energy. The velocity after the elastic and CEX collisions are calculated using conservation equations for linear momentum and energy.

$$\mathbf{v_1^*} = \frac{m_1 \mathbf{v_1} + m_2 \mathbf{v_2}}{m_1 + m_2} + \frac{m_2}{m_1 + m_2} \mathbf{v_r^*} \tag{3}$$

$$\mathbf{v_2^*} = \frac{m_1 \mathbf{v_1} + m_2 \mathbf{v_2}}{m_1 + m_2} - \frac{m_2}{m_1 + m_2} \mathbf{v_r^*} \tag{4}$$

The post-collision relative velocity, $\mathbf{v_r^*}$, given in Eqs. (3) and (4) is determined by the center of mass deflection angle, χ, and azimuth angle, γ, and angles α and β specifying the direction of initial velocity vector with respect to the inertial coordinate system.

$$\mathbf{v_r^*} = v_r \begin{pmatrix} \sin \chi \cos \gamma \\ \sin \chi \sin \gamma \\ \cos \chi \end{pmatrix}^T \begin{bmatrix} \cos \alpha \cos \beta & -\sin \alpha & \cos \alpha \sin \beta \\ \sin \alpha \cos \beta & \cos \alpha & \sin \alpha \sin \beta \\ -\sin \beta & 0 & \cos \beta \end{bmatrix} \begin{pmatrix} \hat{x} \\ \hat{y} \\ \hat{z} \end{pmatrix} \tag{5}$$

Given the pre-collision velocities of both incident and target particles, the post-collision velocities of the two particles can be calculated using Eqs. (4) and (5) once χ and γ are determined. Because any value for γ is equally probable, γ is chosen simply by $\gamma = 2\pi(\text{rand}\#)$. Similarly, b is determined with random number generator, $b = \sqrt{\text{rand}\#}$, and corresponding value for χ is calculated from deflection function described in the next section.

B. Deflection Function

In order to determine χ, a priori knowledge of the functional form or the relationship between χ and impact parameter, b, is required. Scharfe et al.[14] formulated functional forms of differential cross sections, $d\sigma/d\chi$, for the elastic and CEX collisions based on the empirically determined differential cross section,[15] $d\sigma/d\Omega$, for primary xenon ion energy of 300 eV. The relationship between χ and b can be deduced, using a cumulative distribution function. When the background pressure exceeds 0.44 mTorr, mean free path becomes smaller than the length of the test cell, and particles encounter neutrals more than once on average before reaching the exit plate electrode. Every time high energy particles elastically collide with background neutrals, energy is transfered to the target neutrals, and the incident particle energy is reduced. Therefore, it is necessary to use a

Figure 3. Classical scattering trajectory

model that allows determination of the deflection angle for any ion energy less than 1500 eV. The empirical model formulated by Scharfe et al.[14] can not be applied in this situation as the empirical model does not cover the range of ion energies. Scattering of ions and neutrals due to elastic collisions with background
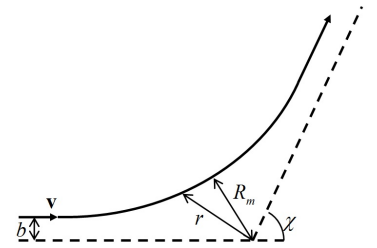
American Institute of Aeronautics and Astronautics

neutrals are determined using a combination of two elastic collision models: classical scattering model with repulsive interaction potential[7] and variable hard sphere (VHS) model,[16] depending on species and its energy. Scattering of secondary electrons by background neutrals is approximated by hard sphere model, in which, physical cross section is used where $\sigma_{eo} = \pi d_o^2/4$. Referring to figure 3, the center of mass deflection angle can be calculated by the classical approach.[17] In this approximation, an appropriate functional form of interaction or intermolecular potential, $V(r)$, has to be chosen in order to predict the scattering angles.

$$\chi(b, E_r) = \pi - 2b \int_{R_m(b,E_r)}^{\infty} \frac{dr}{r^2[1 - b^2/r^2 - V(r)/E_r]^{\frac{1}{2}}} \tag{6}$$

Here, $E_r = 1/2 m_r v_r^2$ and $m_r = m_1 m_2/(m_1 + m_2)$. The classical turning point or the minimum distance of approach, R_m, is calculated by finding the largest root of the equation.

$$1 - b^2/R_m^2 - V(R_m)/E = 0 \tag{7}$$

At the high energies, the scattering is mostly affected only by the repulsive part of the interaction potential.[7] The potential function used for high energy ions is as follows,

$$V(r) = (27.21 eV)\left(\frac{2.11\text{Å}}{r}\right)^{6.57} \tag{8}$$

At energies below a few eV, the VHS model is used.[16] In this model, the scattering is determined in the same way as hard sphere model while the cross section is determined by Eq. (1) instead of using the physical cross section. The deflection angle is given by the following equation.

$$\chi(b, E_r) = 2\cos^{-1}(b/b_{max}(E_r)) \tag{9}$$
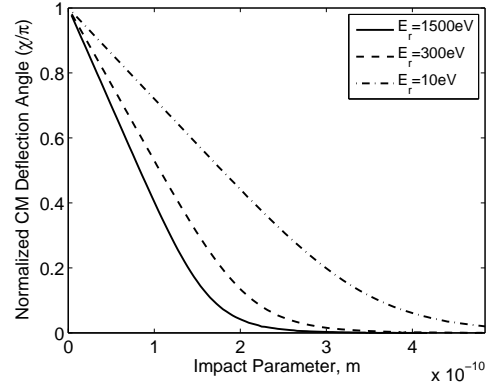
Figure 4. Deflection function for classical scattering with repulsive interaction potential.

Figure 4 shows the center of mass deflection angle as a function of impact parameter. The center of mass scattering angle approaches zero as $b \to 0$, however, it never actually reaches zero. This implies that the total collision cross-section is unbounded. In applying the model, it is necessary to provide a cut-off impact parameter or the deflection angle.[16] For this computational effort, the cut-off or the maximum impact parameters, b_{max}, are chosen from σ_{el} for corresponding energies. Figures 5 and 6 compare $\chi(b, E_r)$ obtained from the two models used in the simulation for ion energy of 300 eV. Figures 5 and 6 also show the deflection functions calculated from the empirical model by Scharfe et al.[14] For the VHS model, cumulative probability function is 0.5 at $\chi/\pi = 0.5$, indicating 50% probability in having deflection angle greater or less than 0.5π; this is as expected because the VHS model gives isotropic scattering in the center of mass coordinate. It can be readily seen that the deflection function deduced from the empirical model gives a high probability ($\approx 60\%$) in very small angle scattering ($< 1°$). The deflection function for classical scattering model lies between the VHS model and the function deduced from the empirical model and shows that 50% probability of having less than $18°$ deflection.
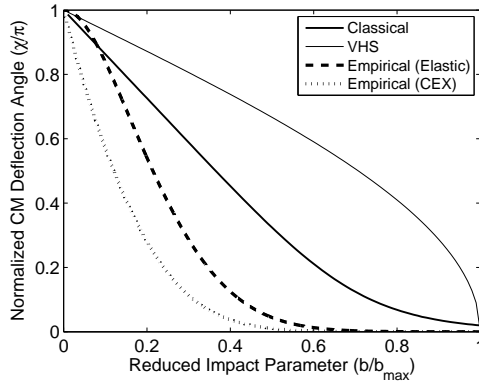
Figure 5. Comparison of deflection functions for ion energy of 300 eV. The impact parameter is normalized by $b_{max} = 2.92$Å.
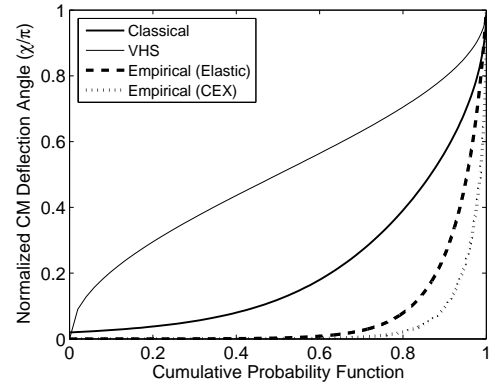
Figure 6. Deflection angle as a function of cumulative probability

American Institute of Aeronautics and Astronautics

C. Differential Cross-Section

Using the scattering angle in the center of mass frame, differential cross-section can be derived.

$$\left.\frac{d\sigma(\chi)}{d\Omega}\right|_{CM} = \left|\frac{b}{\sin\chi(d\chi/db)}\right| \tag{10}$$

$d\chi/db$ can be approximated by using first order difference equations. Recently, Chiu et al.[15] measured absolute differential cross-sections, $d\sigma(v)/dv$, for Xe^+ and Xe^{2+} scattered by Xe atoms in their guided ion beam experiment. The measured differential cross-sections as a function of laboratory velocity agreed well with the differential cross-section calculated based on *ab initio* ion-atom interaction potential. Using the interaction potential, the differential cross-section, $d\sigma(\chi)/d\Omega_{CM}$, was computed. In their calculation, the effect of both elastic and charge exchange collision are considered as both collisions affect the current measured at the ion detector in their experiment.

$$\left.\frac{d\sigma_i(\chi)}{d\Omega}\right|_{CM} = (1 - P_{CEX}(\chi))\left.\frac{d\sigma(\chi)}{d\Omega}\right|_{CM} + P_{CEX}(\chi)\left.\frac{d\sigma(\pi - \chi)}{d\Omega}\right|_{CM} \tag{11}$$

The first and second terms on the right-hand side of Eq. (11) donate the elastic and CEX collision contributions of the total differential cross-section, respectively. The charge exchange probability, P_{CEX}, is highly oscillatory, ranging between 0 and 1 when deflection angle is greater than some critical value (typically 1° for symmetric CEX collision[15]). Eq. (11) can be simplified by using an average value of 0.5. This assumption lead to the use of the relationship $\sigma_{el} = \sigma_{CEX} = \frac{1}{2}\sigma_i$ as mentioned above. The same transformation is performed to compare the differential cross sections obtained by Chiu et al.[15] and classical scattering by repulsive potential. If the collision partners have equal mass, the center of mass differential cross sections can be converted into the laboratory reference frame with the following equation.

Figure 7. Laboratory frame differential cross sections for ion energy of 300 eV

$$\left.\frac{d\sigma}{d\Omega}\right|_{LAB} = \left.\frac{d\sigma}{d\Omega}\right|_{CM} 4\cos(\chi/2) \tag{12}$$

For the CEX collision, the laboratory differential cross section is calculated by replacing χ with $\pi - \chi$ in Eq. (12). Figure 7 plots LAB differential cross sections derived using classical scattering with repulsive potential and the empirical model[14] for ion energy of 300 eV. For the classical scattering model, the cut-off deflection angle, θ_{cutoff}, that corresponds to $b/b_{max} = 1$ is 1.75 degrees. At angles smaller than θ_{cutoff} or greater than $\pi/2 - \theta_{\text{cutoff}}$, the differential cross section drops to a very small values whereas the curve fit to empirically determined $d\sigma/d\Omega$ gives a large values past the cut-off angles. The high probability of scattering at very small angles shown in figure 6 is strongly affected by the large differential cross section at a deflection angle very close to 0 or $\pi/2$, causing high probability of deflection at very small scattering angles.
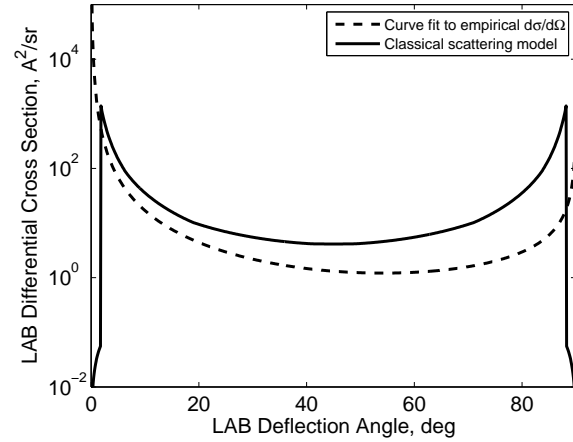
III. Analytical Model for Downstream Current

A flux Γ' of the beam ions traveling a distance of dx can be expressed in terms of initial flux Γ, neutral density n_o, and the total collision cross-section σ.[18]

$$\Gamma' = \Gamma(1 - n_o\sigma dx) \tag{13}$$

Then, the change of Γ with distance is

$$\frac{\Gamma' - \Gamma}{dx} = \frac{d\Gamma}{dx} = -n_o\sigma\Gamma \tag{14}$$

American Institute of Aeronautics and Astronautics

Integrating Eq. (14), ion beam current at any distance, x, is calculated.

$$J = J_0 \exp(-n_o \sigma x) \tag{15}$$

where J is given as $J = e\Gamma A$. Eq. (15) can be used to predict the total current measured at the collector plate. If it is assumed that ions experiencing elastic collisions are deflected at large enough angles, then the cross section in Eq. (15) is simply $\sigma = \sigma_i$. However, the deflection functions given in section II predict higher probability of small angle scattering due to elastic collisions. Therefore, the analytical model predicts lower total current at the exit orifice.

IV.   Results and Discussion

Figure 9 shows sum of currents at the back aperture and the collector plate, measured in the ion beam experiment and predicted by the computational and the analytical models. It can be seen in figure 9 that the two models agree fairly well with the experimental result. At very low pressure, most of the primary ions go straight into the exit orifice. As the pressure is increased, a fraction of ions start to diverge from the beam because of the elastic and CEX collisions, and the current reaching the exit orifice is decreased exponentially as predicted by Eq. (15). Even when ions collide with neutrals elastically, the primary ions can reach the exit orifice if the deflection angle is small enough. The analytical model predicts lower currents going through the exit orifice because the model neglects the primary ions scattered at very small angles.

Figure 8. Total current measured at all the electrodes during ion beam experiment[1]

Figures 10 and 11 plot currents measured during the ion beam experiment and predicted by the computational model at the inner cylinder wall and the exit plate, respectively. Based on the collision model used in the simulation, the majority of currents measured at the exit plate is due to the primary ions colliding with background neutrals and scattering at sufficiently small angles. The CEX ions, in addition to the primary ions with larger scattering angle, contribute to the current measured at the inner cylinder electrode since the CEX ions are likely to have large deflection angles. As shown in figure 10, the electrode current increases with increasing test cell pressure up to 1 mTorr and decreases gradually at larger pressure. The initial increase is due to the rapid rise in the CEX collision probability. Past the test pressure of about 1 mTorr, the probability of ion beam experiencing collision reaches 90%, and further increasing the test pressure would not change the collision probability significantly. The decrease in the inner cylinder current above the test cell pressure is rather due to the reduction in the total current going into the test cell, as shown in figure 8, caused by neutrals coming out the test cell blocking the beam during the ion beam experiment. The computational model predicts a higher inner cylinder current past the pressure of 1 mTorr compared to the measured current during the experiment. The discrepency is also seen in the exit plate current. Exit plate current decreases past the pressure of 1 mTorr whereas almost constant exit plate current is measured during the ion beam experiment. At test cell pressure greater than about 0.44 mTorr, collision mean free path is equal to the length of the test cell. Therefore, the difference between the simulation and the experiment becomes significant when a particle experiences multiple collisions. Every time an incident primary ions elastically collide with background neutrals without exchanging a charge, the kinetic energy of the ions is transfered to the target neutrals since the velocity of the incident ions is much (two orders of magnitudes) greater than that of the target neutrals. The classical scattering with repulsive potential predicts high probability in small angle scattering, however, large angle scattering is still possible. In the case of large angle scattering, the incident ion energy can be reduced significantly below the initial energy. The classical scattering with the interaction potential used in the model is a good approximation only at high energies,[7] thus, a more accurate interaction potential function which is valid for wider range of ion energies is needed to be implemented. Moreover, the gap between the experimental and the computational
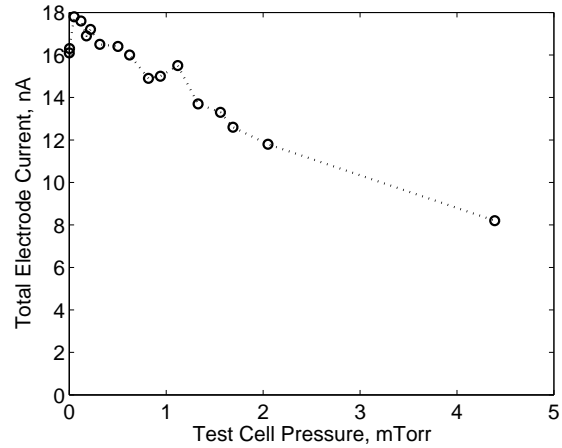
American Institute of Aeronautics and Astronautics

results is greatly affected by the deflection function for the CEX collisions. In the computational model, it is assumed that half of collisional event involves charge exchange event so that $\sigma_{CEX} = 0.5\sigma_{total}$. At test cell pressure of 1.32 mTorr, three collision events take place on average before the primary ions get to the downstream end of the test cell. This means that, out of all the ions impacting any electrode, a fraction of $(0.5^3 =)0.125$ is due to the primary ions experiencing elastic collisions without charge exchange whereas a fraction of $(1 - 0.125 =)0.875$ is due to the CEX ions. In approximating CEX collision event, it is assumed the same deflection function for the elastic and CEX collisions. However, this assumption may not be appropriate as the differential cross section is assymeteric as shown in figure 7. In figures 9 to 11, it can be seen that the secondary electrons contribute to the electrode currents significantly, reducing the discrepancy between the experimental and the computational results. The secondary electron emissions from surface are primarily caused by the high energy primary ions and neutrals, and the electron current emitted from electrodes is proportional to the ion and neutral currents impacting the electrodes. As a result of the CEX collisions, the incident ions deflected at small angles receive electrons from the target neutrals and become high energy neutrals. A large fraction of the fast neutrals impacts the exit plate as well as the primary ions, thus, significant number of electrons are emitted from the exit plate, increasing the exit plate current as they leave and reducing the inner cylinder current as they impact.
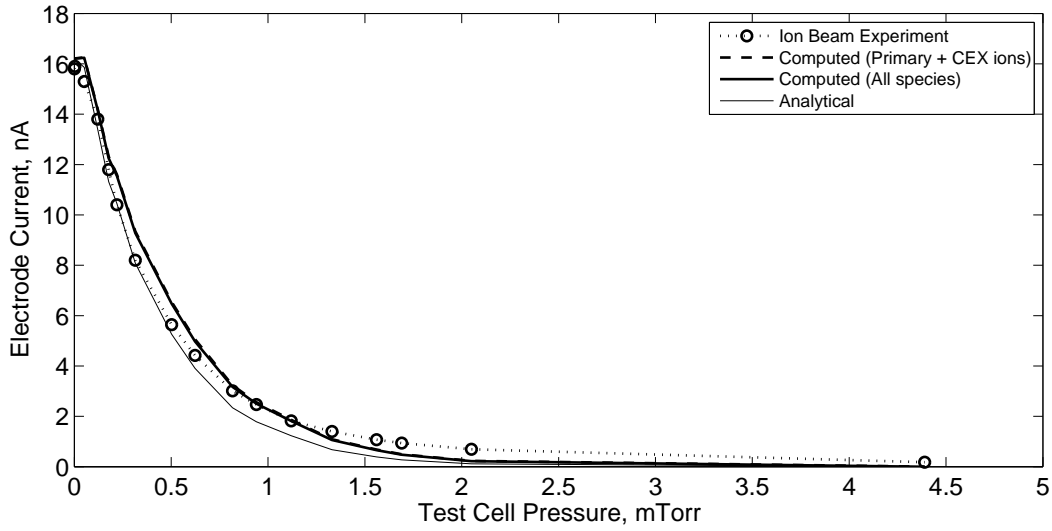

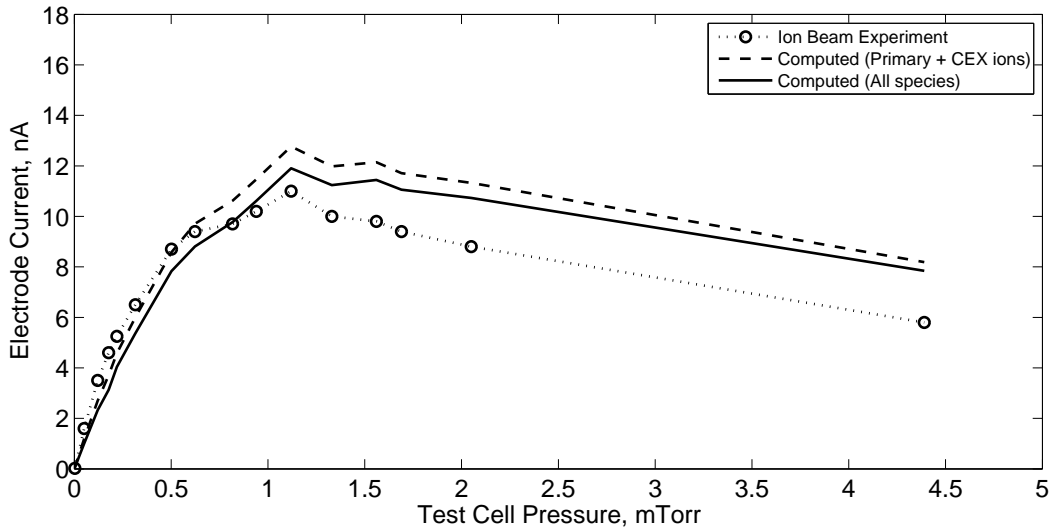Figure 9. Electrode current at back aperture and collector plate

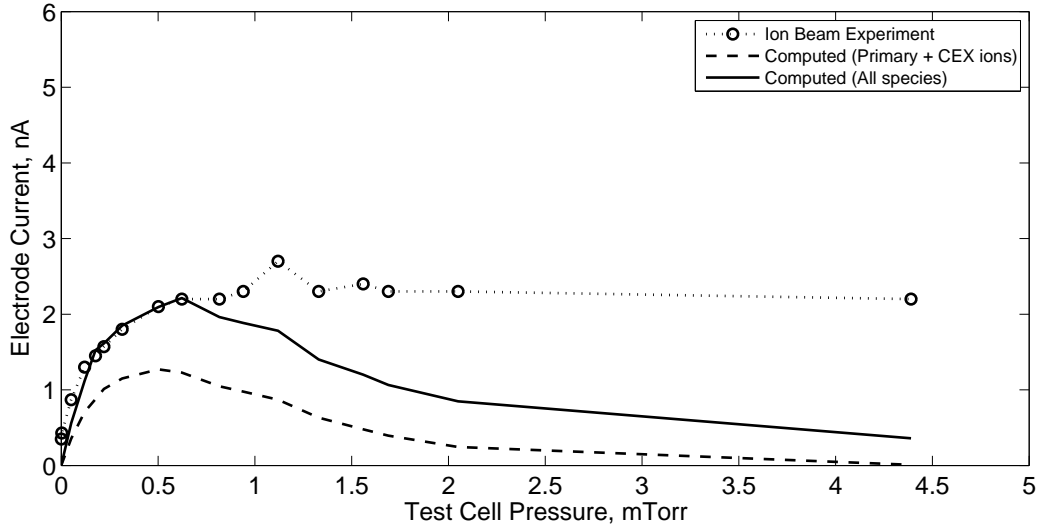Figure 10. Electrode current at inner cylinder

American Institute of Aeronautics and Astronautics

Figure 11. Electrode current at exit plate

V. Conclusion

A PIC Monte Carlo collision model is implemented to investigate the dominant collisional effects on plasmas during the ion beam experiment. The collision mechanisms implemented in the simulation are the elastic and CEX collisions. The scattering due to the two types of collisions is approximated by the classical scattering model with repulsive interaction potential. Poisson's equation is solved computationally to calculate the electric potential in the computational domain. Four different species (Primary and CEX ions, fast neutrals, and secondary electrons) are tracked separately based on the electric potential, and their destinations are computed. The currents at different electrodes predicted by the simulation are compared with the ion beam experiment.

The simulation result agrees fairly well with the experiment up to test cell pressure of 1 mTorr; below the test cell pressure, each primary ion experiences one or two collisions on average. Multiple collisions are involved at a higher pressure, and the simulation result starts to digress from the experimental result. The discrepancy is thought to be due to the collision model used in the simulation. The classical scattering model with repulsive intermolecular potential is only a good approximation at high ion energies while the primary ion energies can be reduced significantly from the initial energy after experiencing many collisions.

In order to improve the model, *ab initio* ion-atom interaction potential, recently verified by Chiu et al.,[15] should be considered for implemention instead of only using repulsive part of the interaction potential. In addition to the classical scattering model, a better model in approximating the CEX collision event is needed to be implemented. Furthermore, there are a few more parts of the simulation model to be improved; they are extending the computational domain to include front and back apertures, using beam profile and divergence angle observed in the experiment, and improving the secondary electron sub-model.

Acknowledgements

References

[1] Wirz, R., Chu, L., Patino, M., and Mao, H., "Well-Characterized Plasma Experiments for Validation of Computational Models," *47th AIAA/ASME/SAE/ASEE Joint Propulsion Conference, San Diego, CA, July 31-August 3*, 2011 (to be published).

[2] Vincenti, W. G. and Kruger, C. H., *Introduction to Physical Gas Dynamics*, Krieger Publishing Company, Malabar, Florida, 1965.

[3] Oh, D., "Computational modeling of expanding plasma plumes in space using a PIC-DSMC algorithm," *Ph.D. Dissertation, Aeronautics and Astronautics Dept., Massachusetts Institute of Technology*, 1997.

[4] Brophy, J., Katz, I., Polk, J., and Anderson, J., "Numerical simulations of ion thruster accelerator grid erosion," *38 th Joint Propulsion Conference, Indianapolis, IN, July 7-10*, 2002, pp. 1–12.

[5] Wirz, R., Anderson, J. R., Goebel, D. M., and Katz, I., "Decel Grid Effects on Ion Thruster Grid Erosion," *IEEE Transactions on Plasma Science*, Vol. 36, No. 5, Oct. 2008, pp. 2122–2129.

[6] Anderson, J., Katz, I., and Goebel, D., "Numerical simulation of two-grid ion optics using a 3D code," *40th AIAA Joint Propulsion Conference, Fort Lauderdale, Florida, July 12-14*, 2004.

[7] Mikellides, I., Katz, I., Kuharski, R., and Mandell, M., "Elastic Scattering of Ions in Electrostatic Thruster Plumes," *Journal of Propulsion and Power*, Vol. 21, No. 1, Jan. 2005, pp. 111–118.

[8] Varga, P. and Winter, H., *Particle Induced Electron Emission II. In: G. Hohler, Editor, Springer Tracts in Modern Physics Vol. 123*, Springer, Berlin, 1992.

[9] Lakits, G., Arnau, A., and Winter, H., "Slow-particle-induced kinetic electron emission from a clean metal surface: A comparison for neutral and ionized projectiles," *Physical Review B*, Vol. 42, No. 1, July 1990, pp. 15–24.

[10] Alonso, E., Alurralde, M., and Baragiola, R., "Kinetic electron emission from solids induced by slow heavy ions," *Surface Science*, Vol. 166, No. 2-3, 1986, pp. L155–L160.

[11] Birdsall, C. K. and Langdon, A. B., *Plasma Physics via Computer Simulation*, McGraw-Hill, New York, 1991.

[12] Ruyten, W., "Density-Conserving Shape Factors for Particle Simulations in Cylindrical and Spherical Coordinates," *Journal of Computational Physics*, Vol. 105, No. 2, April 1993, pp. 224–232.

[13] Miller, J. S., Pullins, S. H., Levandier, D. J., Chiu, Y.-h., and Dressler, R. a., "Xenon charge exchange cross sections for electrostatic thruster models," *Journal of Applied Physics*, Vol. 91, No. 3, 2002, pp. 984.

[14] Scharfe, M. K., Koo, J., and Azarnia, G., "DSMC Implementation of Experimentally-Based $Xe^+ + Xe$ Differential Cross Sections for Electric Propulsion Modeling," *AIP Conf. Proc. 27th International Symposium on Rarefied Gas Dynamics, May 20*, Vol. 298, 2011, pp. 1085–1090.

[15] Chiu, Y.-H., Dressler, R. a., Levandier, D. J., Houchins, C., and Ng, C. Y., "Large-angle xenon ion scattering in Xe-propelled electrostatic thrusters: differential cross sections," *Journal of Physics D: Applied Physics*, Vol. 41, No. 16, Aug. 2008, pp. 165503.

[16] Bird, G. A., *Molecular Gas Dynamics and the Direct Simulation of Gas Flows*, Clarendon Press, Oxford, 1994.

[17] Child, M. S., *Molecular Collision Theory*, Academic Pres Inc., London, 1974.

[18] Chen, F. F., *Introduction to Plasma Physics and Controlled Fusion Volumn 1: Plasma Physics*, Springer, New York, 2nd ed., 2006.